SP-MoMamba: Superpixel-driven Mixture of State Space Experts for Efficient Image Super-Resolution

Anonymous authors
Paper under double-blind review

Abstract

The state space model (SSM) has garnered significant attention recently due to its exceptional long-range modeling capabilities achieved with linear-time complexity, enabling notable success in efficient super-resolution. However, applying SSMs to vision tasks typically requires scanning 2D visual data with a 1D-sequence form, which disrupts inherent semantic relationships and introduces artifacts and distortions during image restoration. To address these challenges, we propose a novel SP-MoMamba method that integrates SSMs with the semantic preservation capability of superpixels and the efficiency advantage of Mixture-of-Experts (MoE). Specifically, we pioneer the use of superpixel features as semantic units to reconstruct the SSM scanning method, proposing the Superpixel-driven State Space Model (SP-SSM) as a basic building block of SP-MoMamba. Furthermore, we introduce the Multi-Scale Superpixel Mixture of State Space Experts (MSS-MoE) scheme to strategically integrate SP-SSMs across scales, effectively harnessing the complementary semantic information from multiple experts. This multi-scale expert integration significantly reduces the number of pixels processed by each SSM while enhancing the reconstruction of fine details through specialized experts operating at different semantic scales. This framework enables our model to deliver superior performance with minimal computational overhead.

1 Introduction

Single-image super-resolution (SR) is a pivotal technique in image processing, aimed at reconstructing high-resolution (HR) images from their low-resolution (LR) counterparts to enhance image detail and visual quality. This technology finds widespread application across diverse fields, including medical imaging, surveillance systems, and satellite imagery. Numerous studies have leveraged convolutional neural networks (CNNs) Dong et al. (2015); Lim et al. (2017); Zhang et al. (2018) and Transformer Liang et al. (2021); Li et al. (2023b); Zhou et al. (2023) to learn this inherently ill-posed mapping relationship. However, most SR methods Lim et al. (2017); Zhang et al. (2018) relied on deeper and more complex architectures to achieve superior performance. These methods often entail high computational complexity, rendering real-time processing impractical on resource-constrained devices and thereby limiting their deployment and widespread adoption in real-world scenarios. Although some researchers have reduced computational complexity through methods such as neural architecture search Chu et al. (2021), recursive networks Tai et al. (2017), and model distillation Liu et al. (2020); Hui et al. (2018), these efforts have not yet fully addressed this issue.

Recently, state space models (SSMs), exemplified by Mamba Gu & Dao (2023), have opened new avenues for Efficient SR. Mamba offers linear computational complexity and excels at modeling long sequences, initially proving its value in high-level vision tasks such as image classification Liu et al. (2024); Zhu et al. (2024) and object detection Zhang et al. (2025a); Wang et al. (2024c). On this basis, researchers adapted Mamba for low-level vision tasks like image denoising Guo et al. (2024), image SR Qiao et al. (2024), and low-light image enhancement Zou et al. (2024); Zhen et al. (2024). For example, MambaIR Guo et al. (2024), based on visual SSM framework, achieved reconstruction quality comparable to transformer-based methods while maintaining lower computational costs. These developments demonstrate that Mamba effectively balances performance and

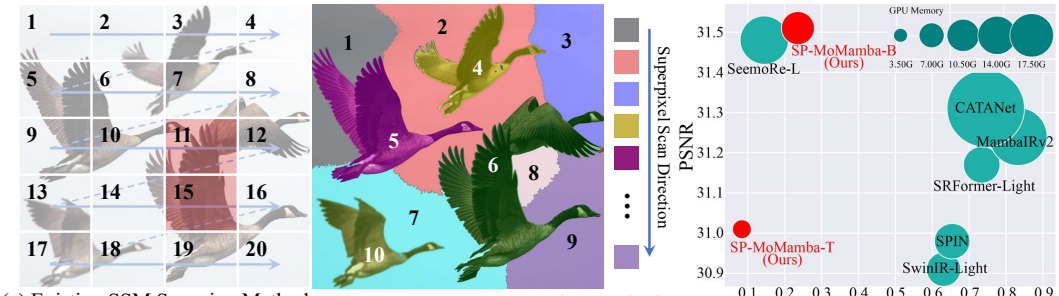

(a) Existing SSM Scanning Method
× semantic information is disrupted
× high cost and redundancy full scanning

(b) Our MSS-MoE Scanning Method
✓ stronger semantic information
✓ only a few pixel needed scanning

(c) Efficiency Comparison

Figure 1: (a) The existing method Guo et al. (2024) suffers from the adverse effects of the scanning method of Mamba (the multi-directional scans are not shown for presentation clarity). (b) The proposed MSS-MoE scanning method can efficiently model the global information by a mixture of experts at different scale, and embed the semantic consistency of superpixels into Mamba. (c) Comparison between performance vs Inference times and GPU Memory on Manga109 ×4 dataset. Inference times and GPU Memory are calculated on 720p HR image.

efficiency in Efficient SR, though additional optimizations are still required to tailor it to specific use cases and achieve an ideal performance-efficiency trade-off.

The main challenge of Mamba-based SR methods currently is the inability to maintain correct semantic relationships during global image scanning. **Specifically, these methods convert 2D images into 1D sequences during the scanning process, which disrupts inherent semantic information and impairs SR model performance.** As shown in Figure 1 (a), this unfolding process destroys the semantic connections between spatially adjacent pixels (e.g., vertically neighboring pixels), hindering the model's ability to capture local structural details effectively. Although strategies such as multi-directional scanning Guo et al. (2024) or cascaded Mamba Qiao et al. (2024) modules attempt to mitigate this issue, they fail to address the fundamental problem of semantic disruption, instead exacerbating computational overhead and parameter complexity. Furthermore, **repetitive textures in natural images, such as skies and water surfaces, are prone to semantic confusion in 1D sequences, weakening the model's grasp of overall image structure.** This shows that there is still much room for improvement in the processing efficiency and semantic preservation of the current Mamba-based method.

To address the above challenges, we propose SP-MoMamba, an efficient SSM tailored for efficient SR. Given that superpixel features naturally delineate distinct semantic regions, as shown in Figure 1 (b), our core innovation lies in integrating their semantic preservation capabilities into a SSM framework. Technically, our SP-MoMamba is composed of stacked Layers of Experts (LoEs) for dynamically selecting the pivotal features via experts, focusing on two different aspects. At the macro level, each LoE contains two consecutive expert blocks: (a) *Superpixel Global Modulating Expert* (SGME), which excels in modeling global semantic information, and (b) *Local Spatial Modulating Expert* (LSME), which is proficient in efficient reconstruction of local spatial details. At the micro level, we design a Multi Scale Superpixel Mixture of State Space Experts (MSS-MoE) as the foundational component of SGME, which dynamically selects the optimal scale of superpixel-driven state space model (SP-SSM) for different inputs at different scales, to accurately capture the correlation between global semantics. Specifically, SP-SSM compresses semantically homogeneous features into superpixel units through superpixel sampling. Then, SSM calculates the similarity between superpixels. This similarity is propagated to the corresponding semantic regions to enhance consistency within the regions. Overall, our method obtains different professional knowledge by explicitly mining experts of different granularity for different expertise, thereby accurately reconstructing more details. Our contributions are summarized below:

- To the best of our knowledge, SP-MoMamba is the first work that pioneers the use of superpixel features as fundamental semantic units to restructure the input for State Space Models (SSMs). We correspondingly introduce a Superpixel-driven State Space Model (SP-SSM), which effectively resolves the issue of semantic disruption inherent in the scanning process of Mamba-based methods.

- We propose a Multi-Scale Superpixel Mixture of State Space Experts (MSS-MoE), enabling comprehensive global modeling by dynamically selecting optimal experts across scales to leverage semantic similarities.
- Quantitative comparisons in Figure 1 (c) further confirm the advantages of our method: it surpasses other efficient SR techniques in reconstruction fidelity and achieves a significant reduction in inference time.

2 Related Works

Efficient Super-resolution Methods. Efficient super-resolution methods have been pursued through lightweight architectures Ahn et al. (2018); Hui et al. (2018); Sun et al. (2023) and efficient transformers Zhang et al. (2022); Lu et al. (2022); Zou et al. (2022). CARN Ahn et al. (2018) uses cascading for feature integration, IMDN Hui et al. (2018) employs feature distillation, and SAFMN Sun et al. (2023) builds channel-aware pyramids. To reduce Transformer complexity, methods like ELAN Zhang et al. (2022) and ESRT Lu et al. (2022) lower dimensionality, while SCET Zou et al. (2022) uses pixel attention. Recently, SPIN Zhang et al. (2023) leverages superpixel and cross-attention. However, balancing efficiency and performance remains challenging.

Recently, Mamba Gu & Dao (2023), a selective SSM, has been successfully adapted to the vision domain, such as VMamba Liu et al. (2024) and VIM Zhu et al. (2024). Subsequently, its application has been further explored in low-level vision tasks, yielding a variety of methods Zhen et al. (2024); Zou et al. (2024) with promising results. MambaIR Guo et al. (2024), for instance, captures spatial information and enhances channel interactions. However, these Mamba-based methods rely on multi-directional scanning to process all pixels, disrupting semantic coherence and increasing computation. In contrast, our approach uses superpixels to extract compressed semantic features, modeling their spatial relationships with SSMs, preserving semantics while significantly reducing complexity.

Mixture of Experts (MoE). Recently, the Mixture of Experts (MoE) method has gained widespread adoption in large-scale language models due to its efficiency and scalability. Thus, MoE has been extended to advanced vision tasks, including image classification Riquelme et al. (2021), object detection Wu et al. (2022), as well as low-level vision tasks Emad et al. (2022); Zamfir et al. (2024); Rossi et al. (2025). For example, literature Emad et al. (2022) and Liang et al. (2022) extract latent degradation features to construct MoE-based adaptive networks, effectively addressing diverse degradation patterns in blind SR. SeemoRe Zamfir et al. (2024) employs rank-modulated experts to prioritize features with the highest information content, followed by spatial modulation experts to achieve precise spatial enhancement. Similarly, Swin2-MoSE Rossi et al. (2025) enhances Swin2SR Conde et al. (2022) by incorporating an MoE framework, yielding improved visual outcomes. While these methods leverage the flexibility and efficiency of MoE to achieve commendable performance, there remains potential for further improvement in image quality.

3 Motivation

To extend state space models (SSMs) from 1D sequence data to 2D visual data, most current research Guo et al. (2024); Qiao et al. (2024); Liu et al. (2024) employs a 2D selective scanning mechanism (SS2D) Liu et al. (2024) to capture spatial correlations, as illustrated in Figure 1(a). However, flattening an image into a 1D sequence often disrupts inherent semantic relationships. For example, two geese that are spatially adjacent in Figure 1(a) might end up widely separated in the 1D sequence, hindering the model's ability to leverage their proximity for semantic inference. Furthermore, images frequently contain repetitive structures like skies and buildings which share similar textures, heightening the risk of semantic confusion. Once unfolded, information from these structures may be incorrectly associated, leading to erroneous predictions. Thus, current SS2D methods struggle to adequately preserve critical spatial structure and semantic information.

Compared to traditional SS2D, which systematically transforms 2D features into 1D sequences, superpixel sampling clusters semantic similar pixels based on color or texture. This effectively reduces the number of pixels requiring processing while maintaining the image's spatial structure and semantic integrity. Therefore, integrating superpixel algorithms into SSMs provides a robust solution to the limitations of conventional SSMs when processing 2D images.

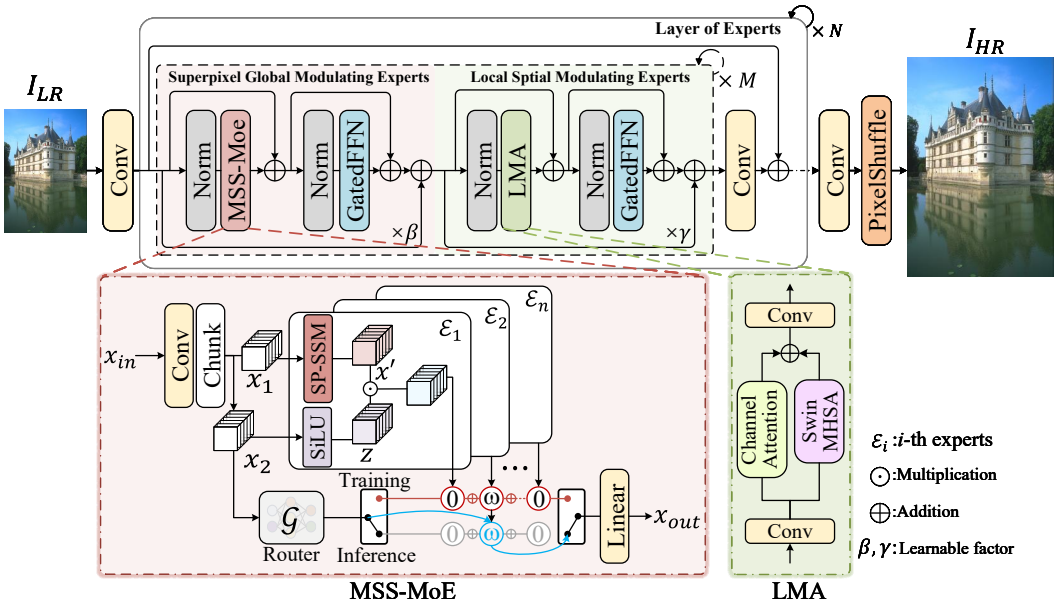

Figure 2: Architecture of our proposed method. SP-MoMamba is composed of several Layer of Experts (LoEs). Each LoE is composed of a superpixel global modulation expert (SGME) and a local spatial modulation expert (LSME). SGME uses multi-scale superpixel mixture of state space experts (MSS-MOE) to select the optimal semantic correlation to refine the global texture, while LMSE uses local mixed attention (LMA) to further restore the local texture.

To verify the issues of semantic interruption in Mamba based methods, we analyze the Local Attribute Maps (LAM) and Diffusion Index (DI) presented in Figure 3. As illustrated, traditional methods like MambaIR and MambaIRv2 exhibit restricted activation areas, reflecting the limitations of standard SS2D in capturing long-range correlations within repetitive structures. In contrast, our proposed SP-MoMamba demonstrates significantly broader activation coverage, indicating the successful utilization of non-local, perceptually similar features. This visual evidence is verified quantitatively by the highest DI score of 45.53 (surpassing 43.61 and 41.46), confirming that our superpixel-integrated approach effectively enhances the model's receptive field and maintains semantic integrity. More visual analysis can be found in the Supplementary material.

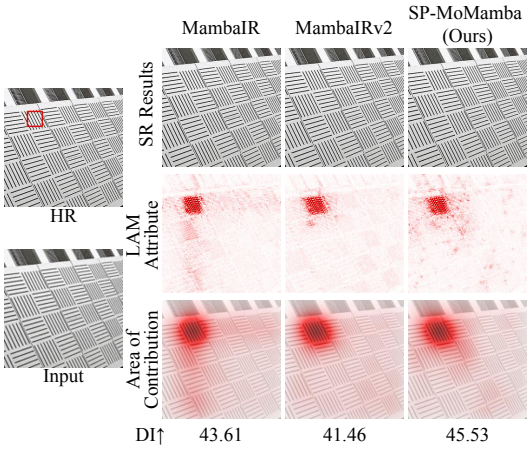

Figure 3: Analysis semantic preservation capability of different methods. The larger the Diffusion Index (DI), the more semantically similar pixels are involved in restoring the corresponding region.

4 METHODOLOGY

In this section, we present our proposed SP-MoMamba, as illustrated in Figure 2. The complete architecture of our pipeline integrates N layers of experts (LoEs) and upsampling layers. Initially, a 3×3 convolutional operation is employed to extract shallow features from the input low-resolution image. These features are then processed through a series of LoEs to recover deep features. Each LoE consists of M paired sets of Superpixel Global Modulating Experts (SGME) and Local Spatial Modulating Experts (LSME), collaboratively enhancing feature restoration. SGME adopts a collaborative reconstruction method by integrating a multi-scale superpixels mixture of state space experts (MSS-MoE), maximizing the interaction of global information. LSME concentrates on refining local features through a localized mixed attention mechanism, which enhances overall performance. In

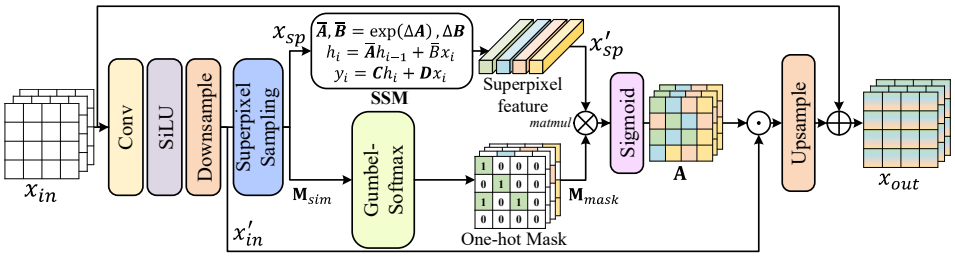

Figure 4: Illustration of the superpixel-driven state space model (SP-SSM). One-hot mask should be $N \times M$, which is converted into a 3D matrix $(H \times W) \times M$ for ease of understanding in the figure.

addition, two residual connections with learnable scales β, and γ are introduced. Finally, the refined deep features are transformed into high-resolution images via a pixelshuffle and convolution.

4.1 Superpixel Global Modulating Experts

Unlike SPIN Zhang et al. (2023) and MambaIR Guo et al. (2024), which rely on substantial computational resources, we prioritize efficiency by constructing global similarity relationships based on interactions among the most relevant scale-specific superpixels. Here, we propose the MSS-MoE, as shown in Figure 2. MSS-MoE employs superpixel-driven state space models (SP-SSMs) at different scales to independently model global features across different resolutions. By leveraging the strengths of the mixture of experts scheme, it selectively integrates the resulting features, ensuring optimal global modeling within each LoE. Then, a Gated Feed-Forward Network (GatedFFN) Chen et al. (2023) is utilized to aggregate contextual information from these global features.

MSS-MoE. As shown in Figure 2, the output features from the last layer normalization serve as the input features x_{in} for this module. A Linear layer is first applied to increase the dimensionality of the feature channels, followed by a split along the channel dimension to yield two distinct features, x_1 and x_2. Subsequently, we employ a SP-SSM module to derive the global attention feature x' from x_1. Meanwhile, x_2 is processed through an activation function to obtain the gating feature z. Consequently, the formulation for each superpixel state space expert is expressed as follows:

$$\mathcal{E}_i(x_1, x_2, s) = x' \odot z = \text{SP-SSM}(x_1, s) \odot \sigma(x_2) \tag{1}$$

where SP-SSM$(\cdot)$ and $\sigma(\cdot)$ denote the SP-SSM module and the SiLU Shazeer (2020) activation function, respectively. The $\odot$ denotes Hadamard product. The s represents the scale parameter of SP-SSM. We employ an SP-SSM to ensure robust modeling of global information while introducing an residual connection to prevent the loss of local information.

However, the SP-SSM operating at a fixed scale may fail to fully exploit all internal information, thereby limiting the model's expressive capacity. To address this, we propose an ensemble approach that integrates superpixel state space experts across multiple scales s_i. A routing network searches the solution space to identify the optimal scale for the superpixel state space experts based on the input and network depth. The final output x_{out} of the MSS-MoE is formulated as follows:

$$x_{out} = \sum_{i}^{n} \mathcal{G}(x_2)\mathcal{E}_i(x_1, x_2, s_i) \tag{2}$$

where $\mathcal{G}(\cdot)$ and $\mathcal{E}(\cdot)$ denote the router function and the i-th expert function, respectively. The s_i represents the scale parameter of the i-th expert's SP-SSM module. Specifically, a router $\mathcal{G}(\cdot)$ is composed of a linear mapping and Softmax to map input features into weights of different superpixel state space experts. The sparsity inherent in the router function $\mathcal{G}(\cdot)$ optimizes computation by assigning greater weights to the top-k superpixel state space experts. During training, our method learns from all superpixel state space experts, while during inference, it utilizes only the selected top-k experts with higher routing weights for computation, thereby enhancing efficiency. Hence, the computational complexity of the inference process becomes independent of the total number of experts, further enhancing efficiency. We further provide the pseudocode for the proposed MSS-MoE in the supplementary materials.

SP-SSM. As shown in Figure 4, given the input feature $x_{in} \in \mathbb{R}^{H \times W \times C}$, we use 3×3 convolution and SiLU activation function to map features. Then, these features are downsampled by a factor of

s, and superpixel sampling is performed to obtain the corresponding M superpixel features $x_{sp} \in \mathbb{R}^{M\times C}$ and similarity matrix $\mathbf{M}_{sim} \in \mathbb{R}^{N\times M}$ (where $N = H \times W$). It is formulated as follows:

$$x_{sp}, \mathbf{M}_{sim} = \text{SPS}(\sigma(\text{Conv}(x_{in})) \downarrow_s) \tag{3}$$

where $\text{SPS}(\cdot)$ denotes the superpixel sampling operation. $\downarrow_s$ represents the downsampling operation by a factor of s. Subsequently, a SSM is employed to perform global information modeling on the superpixel feature x_{sp}, yielding an enhanced superpixel feature $x'_{sp} \in \mathbb{R}^{M\times C}$. The similarity matrix $\mathbf{M}_{sim}$ is transformed into a differentiable one-hot mask $\mathbf{M}_{mask} \in \mathbb{R}^{N\times M}$ using the Gumbel-Softmax Jang et al. (2016) technique applied to log probabilities, enabling the indexing of the most similar superpixel for each pixel. Then, matrix multiplication followed by a sigmoid function is utilized to derive the global attention feature $\mathbf{A} \in \mathbb{R}^{N\times C}$, as follows:

$$x'_{sp} = \text{SSM}(x_{sp}) \tag{4}$$

$$\mathbf{M}_{mask} = \text{Gumbel-Softmax}(\mathbf{M}_{sim}) \tag{5}$$

$$\mathbf{A} = \text{Sigmoid}(\mathbf{M}_{mask} \otimes x'_{sp}) \tag{6}$$

where $\text{Sigmoid}(\cdot)$ and $\otimes$ denote sigmoid function and matrix multiplication. The final output of this module is obtained by multiplying the attention feature $\mathbf{A}$ with x'_{in}, followed by the addition of the original transformed feature x_{in}, as follows:

$$x_{out} = (\mathbf{A} \odot x'_{in}) \uparrow_s + x_{in} \tag{7}$$

Since superpixels encapsulate comprehensive semantic information, the resulting output features effectively capture correlations among distinct semantics.

Superpixel Sampling. We follow the soft k-means-based superpixel algorithm in SSN Jampani et al. (2018) to perform superpixel sampling on images. Given input as $\mathbf{x} \in \mathbb{R}^{N\times C}$ (where $N = H \times W$), M superpixels $\mathbf{s} \in \mathbb{R}^{M\times C}$ and similarity matrix $\mathbf{M}_{sim} \in \mathbb{R}^{N\times M}$ are obtained through T iterations, maximizing their association with the corresponding pixels. Firstly, as shown in Figure 5, we use average pooling to initialize superpixels $\mathbf{s}^0$. Then, we conduct iterations using a similarity matrix that calculates the similarity between each pixel and superpixel. It can be formulated as follows:

$$\mathbf{M}^t_{sim}(i,j) = e^{-||\mathbf{x}(i)-\mathbf{s}^{t-1}(j)||_2^2} \tag{8}$$

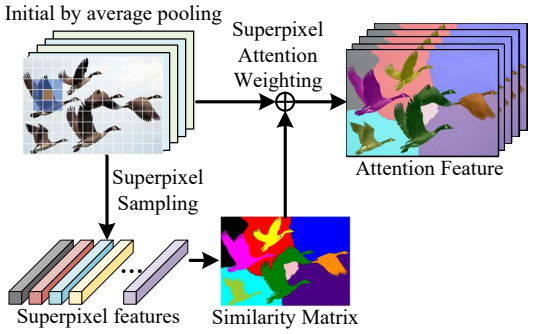

Figure 5: Superpixel sampling of our method, which initializes the superpixel features by average pooling, and then generates the superpixel features and similarity matrix.

Notably, superpixel sampling solely evaluates the similarity mapping between each pixel and its neighboring superpixels. This preserves the local coherence of superpixels, thereby enhancing computational efficiency. Subsequently, we can obtain the superpixel $\mathbf{s}^t$ by computing a weighted sum of all pixels, defined as:

$$\mathbf{s}^t_j = \frac{1}{\mathbf{z}^t(j)} \sum_i \mathbf{M}^t_{sim}(i,j)\mathbf{x}(i) \tag{9}$$

where $\mathbf{z}^t(j) = \sum_i \mathbf{M}^t_{sim}(i,j)$ denotes the normalization term along the column. After T iterations, we can obtain the final similarity matrix $\mathbf{M}^T_{sim}$ and superpixels $\mathbf{s}^T$. Using the similarity matrix, we can assign each pixel to its most similar superpixel, thus generating the corresponding mask, as depicted in Figure 5. Therefore, with the superpixels and their respective masks, we can perform superpixel-based attention weighting on pixels across distinct regions. Our proposed SP-SSM utilizes this critical insight by employing a SSM to assign weights to superpixels, enabling weighted processing of semantic information across distinct regions.

4.2 Local Spatial Modulating Experts

After the proposed MSS-MoE primarily leverages superpixels to capture global semantic relationships, we enhance its capability by incorporating Local Spatial Modulation Experts (LSME) to

strengthen the processing of local information. Given that MSS-MoE requires scanning only a limited number of superpixels, this property is insufficient for the modeling of local correlation. Consequently, we adopt a robust combination of shift window-based multi-head self-attention (SWin-MHSA) and channel attention to construct a Local Mixed Attention Module (LMA), as depicted in Figure 2. Channel attention recalibrates features across channels to emphasize salient local information; subsequently, Swin-MHSA captures fine-grained spatial dependencies within local windows. GatedFNN then refines features by integrating global and local information, preserving prior semantics while enhancing detail capture, thus improving overall model performance.

Scale	Model	Params (M)↓	GMACs↓	Set5		Set14		BSD100		Urban100		Manga109	
				PSNR↑	SSIM↑	PSNR↑	SSIM↑	PSNR↑	SSIM↑	PSNR↑	SSIM↑	PSNR↑	SSIM↑
×2	CARN-M	412K	91	37.53	0.9583	33.26	0.9141	31.92	0.8960	31.23	0.9193	—	—
	PAN	261K	71	38.00	0.9605	33.59	0.9181	32.18	0.8997	32.01	0.9273	38.70	0.9773
	DRSAN	370K	86	37.99	0.9606	33.57	0.9177	32.16	0.8999	32.10	0.9279	—	—
	SAFMN	228K	52	38.00	0.9605	33.54	0.9177	32.16	0.8995	31.84	0.9266	38.71	0.9771
	FECAN-tiny	107K	24	38.00	0.9605	33.52	0.9172	32.14	0.8993	31.86	0.9252	38.76	0.9772
	SeemoRe-T	220K	45	38.06	0.9608	33.65	0.9186	32.23	0.9004	32.22	0.9286	39.01	0.9777
	SRConvNet	387K	74	38.00	0.9605	33.58	0.9186	32.16	0.8995	32.05	0.9272	38.87	0.9774
	SP-MoMamba-T (ours)	259K	85	**38.16**	**0.9612**	**33.81**	**0.9199**	**32.29**	**0.9011**	**32.48**	**0.9312**	**39.76**	**0.9820**
×4	CARN-M	415K	33	31.92	0.8903	28.42	0.7762	27.44	0.7304	25.62	0.7694	—	—
	PAN	272K	28	32.13	0.8948	28.61	0.7822	27.59	0.7363	26.11	0.7854	30.51	0.9095
	DRSAN	410K	31	32.15	0.8935	28.54	0.7813	27.54	0.7364	26.06	0.7858	—	—
	SAFMN	240K	14	32.18	0.8948	28.60	0.7813	27.58	0.7359	25.97	0.7809	30.43	0.9063
	FECAN-tiny	121K	7	32.08	0.8935	28.58	0.7809	27.57	0.7354	25.96	0.7801	30.33	0.9049
	SeemoRe-T	232K	12	32.31	0.8965	28.72	0.7840	27.65	0.7384	26.23	0.7883	30.82	0.9107
	SRConvNet	382K	22	32.18	0.8951	28.61	0.7359	27.57	0.7359	26.06	0.7845	30.35	0.9075
	SP-MoMamba-T (ours)	271K	22	**32.35**	**0.8970**	**28.77**	**0.7850**	**27.69**	**0.7398**	**26.40**	**0.7939**	**31.01**	**0.9160**

Table 1: Comparison to efficient SR models. PSNR (dB ↑) and SSIM (↑) metrics are reported on the Y-channel. **Best** and second best performances are highlighted. GMACs (G) are computed by upscaling to a 1280 × 720 HR image.

Scale	Model	Params (M)↓	GMACs↓	Set5		Set14		BSD100		Urban100		Manga109	
				PSNR↑	SSIM↑	PSNR↑	SSIM↑	PSNR↑	SSIM↑	PSNR↑	SSIM↑	PSNR↑	SSIM↑
×2	SwinIR-Light	910K	244	38.14	0.9611	33.86	0.9206	32.31	0.9012	32.76	0.9340	39.12	0.9783
	SRFormer-Light	853K	236	38.23	0.9613	33.94	0.9209	32.36	0.9019	32.91	0.9353	39.28	0.9785
	SPIN	497K	320	38.20	0.9615	33.90	0.9215	32.31	0.9015	32.79	0.9340	39.18	0.9784
	CAMixerSR	746K	205	38.23	0.9613	34.00	0.9214	32.34	0.9016	32.95	0.9340	39.32	0.9781
	FECAN-light*	732K	162	38.22	0.9614	34.01	0.9216	32.35	0.9017	32.89	0.9787	39.47	0.9784
	Freqformer*	870K	229	38.26	0.9615	34.02	0.9217	32.34	0.9018	32.94	0.9353	39.47	0.9789
	MambaIR-light	905K	334	38.13	0.9610	33.95	0.9208	32.31	0.9013	32.85	0.9349	39.20	0.9782
	SeemoRe-L	931K	197	**38.27**	**0.9616**	34.01	0.9210	32.35	0.9018	32.87	0.9344	39.49	0.9790
	CRAFT	738K	197	38.23	0.9615	33.92	0.9211	32.33	0.9016	32.86	0.9343	39.39	0.9786
	MambaIRv2-light	774K	286	38.26	0.9615	**34.09**	**0.9221**	32.36	0.9019	**33.26**	**0.9378**	39.35	0.9785
	SP-MoMamba-B (ours)	543K	170	**38.27**	**0.9616**	34.04	0.9219	**32.38**	**0.9022**	32.99	0.9357	**40.18**	**0.9827**
×4	SwinIR-Light	897K	64	32.44	0.8976	28.77	0.7858	27.69	0.7406	26.47	0.7980	30.91	0.9151
	SRFormer-Light	873K	63	32.51	0.8988	28.82	0.7872	27.73	0.7422	26.67	0.8032	31.17	0.9165
	SPIN	555K	90	32.48	0.8983	28.80	0.7862	27.70	0.7415	26.55	0.7998	30.98	0.9156
	CAMixerSR	765K	54	32.51	0.8988	28.82	0.7870	27.72	0.7416	26.63	0.8012	31.18	0.9166
	FECAN-light*	749K	42	32.53	0.8990	28.89	0.7879	27.75	0.7421	26.78	0.8049	31.47	0.9181
	FreqFormer*	889K	55	32.54	0.8991	28.89	0.7879	27.76	0.7425	26.73	0.8023	31.36	0.9178
	MambaIR-light	930K	64	32.42	0.8977	28.74	0.7847	27.68	0.7400	26.52	0.7983	30.94	0.9135
	SeemoRe-L	969K	50	32.51	0.8990	28.92	0.7881	27.77	**0.7428**	26.79	0.8046	31.48	0.9181
	CRAFT	753K	52	32.52	0.8989	28.85	0.7872	27.72	0.7418	26.56	0.7995	31.18	0.9168
	MambaIRv2-light	790K	76	32.51	0.8992	28.84	0.7878	27.75	0.7425	**26.82**	**0.8079**	31.24	0.9182
	SP-MoMamba-B (ours)	559K	46	**32.56**	**0.8992**	**28.93**	**0.7885**	**27.78**	0.7426	26.76	0.8030	**31.51**	**0.9210**

Table 2: Comparison to lightweight SR models. PSNR (dB ↑) and SSIM (↑) metrics are reported on the Y-channel. **Best** and second best performances are highlighted. GMACs (G) are computed by upscaling to a 1280 × 720 HR image. * denote retraining based on equivalent experimental configuration.

5 Experiments

5.1 Experimental Settings

Datasets and Evaluation. Following the previous SR methods Liang et al. (2021); Zamfir et al. (2024), we utilize two widely-used datasets, DIV2K Timofte et al. (2017) and Flickr2K Lim et al. (2017) for training. We assess our method performance on five classical benchmark datasets for SR, Set5 Bevilacqua et al. (2012), Set14 Zeyde et al. (2010), BSD100 Martin et al. (2001), Urban100 Huang et al. (2015), and Manga109 Matsui et al. (2015). We also quantify the effectiveness of our method using the PSNR and SSIM metrics on the Y-channel from the YCbCr color space.

Implementation Details. To thoroughly train the proposed model, we augment the training data by randomly cropping it into 64×64 patches and further augment it through random rotations, horizontal and vertical flips. Consistent with Sun et al. (2022), we use the Adam Kingma & Ba

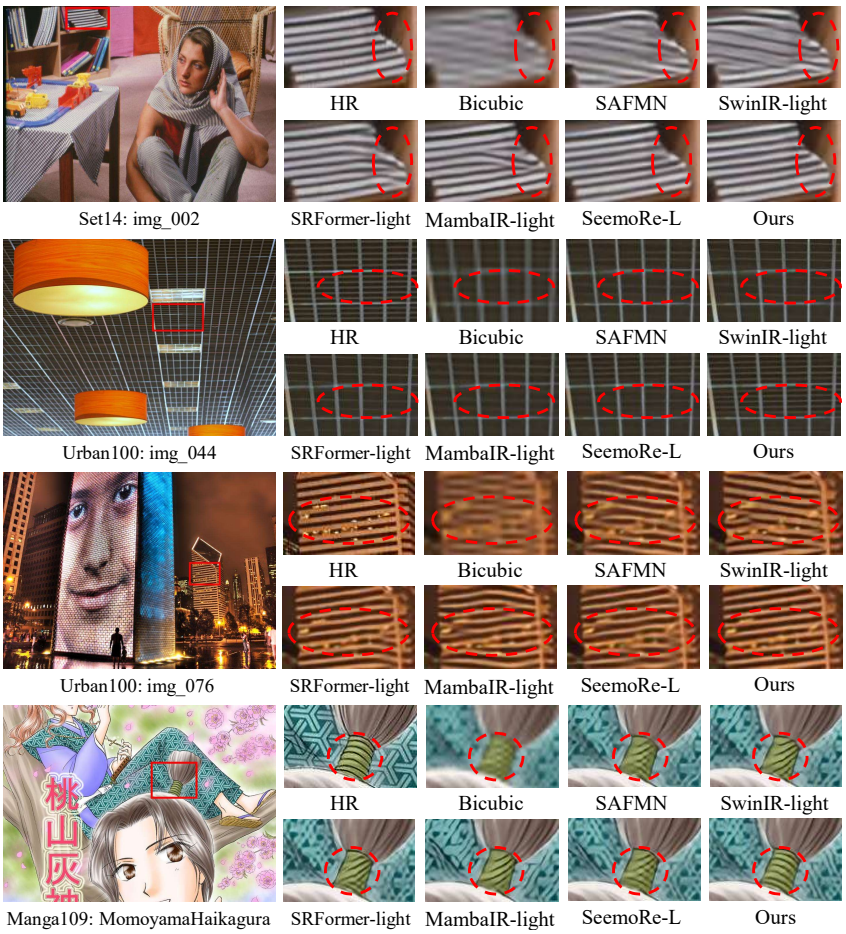

Figure 6: Qualitative comparison of our SP-MoMamba-B with state-of-the-art methods on $4\times$ SR. (Zoom in for the best view)

(2014) optimizer to minimize the L_1 norm between the SR output and the HR ground truth in both pixel and frequency domains across 500K iterations. The batch size is set to 32, with an initial learning rate of 1×10^{-3} which is halved at iterations [250K, 400K, 450K, 475K]. All experiments are implemented using the PyTorch framework and conducted on a single RTX 4090 GPU. We design two variants of the SP-MoMamba model with distinct parameter configurations, denoted as SP-MoMamba-T and SP-MoMamba-B. For all MSS-MoE modules, we configure three experts with downsampling factors of [1, 2, 4]. Further details are provided in the supplementary materials.

5.2 Comparisons with State-of-the-art Methods

Quantitative comparison. We report quantitative results for image SR at $\times 2$ and $\times 4$ scale factors, with comparisons against current efficient state-of-the-art models presented in Table 1, including CARN-M Ahn et al. (2018), PAN Zhao et al. (2020), DRSAN Park et al. (2021), SAFMN Sun et al. (2023), FECAN-tiny Huang et al. (2025), SeemoRe-T Zamfir et al. (2024), SRConvNet Li et al. (2025b). Additionally, we evaluate against lightweight SR models such as SwinIR Liang et al. (2021), SRFormer Zhou et al. (2023), SPIN Zhang et al. (2023), CAMixerSR Wang et al. (2024b), FECAN-light Huang et al. (2025), Freqformer Dai et al. (2024), MambaIR Guo et al. (2024), CRAFT Li et al. (2025a), and MambaIRv2 Guo et al. (2025) in Table 2. Our proposed SP-MoMamba-T stands out as the most efficient method, consistently surpassing all other methods across all benchmarks and scale factors. For instance as clear from Table 1, on Urban100 and Manga109 ($\times 2$), SP-MoMamba-T exceeds SeemoRe-T Zamfir et al. (2024) by 0.26 dB and 0.75 dB, respectively. Scaling our method up to a comparable size with lightweight models yields comparable or superior results. As demonstrated in Table 2, our SP-MoMamba-B exhibits the best PSNR

Method	SSM	SPS	MoE	LMA	GatedFFN	Params	GMACs	BSD100	Urban100
Baseline	-	-	-	-	-	189K	8.4	27.42	25.55
SP-MoMamba-T	✔	-	-	-	-	230K	18.7	27.48	25.64
	✔	✔	-	-	-	197K	16.7	27.54	25.86
	✔	✔	✔	-	-	242K	16.9	27.59	26.07
	-	-	-	✔	✔	211K	16.6	27.61	26.14
	✔	✔	✔	-	✔	261K	19.8	27.63	26.14
	✔	✔	✔	✔	✔	272K	22	27.69	26.40

Table 3: Ablation on key components of SP-MoMamba. We show PSNR results for $\times 4$ upscaling.

performance on average across 5 benchmark datasets. Among them, on Manga109 ($\times 2$), our SP-MoMamba-B outperforms SeemoRe-L Zamfir et al. (2024) and MambaIRv2-light Guo et al. (2025) by 0.69 dB and 0.83 dB, respectively. As demonstrated in Figure 1(c), our SP-MoMamba strikes an optimal balance between performance and efficiency, delivering higher-quality super-resolution results than leading methods while requiring less computational time.

Qualitative comparison. In Figure 6, we compare the visual quality of our method against existing state-of-the-art approaches. As evident from the figure, previous methods often struggle with challenging structural textures, resulting in distortions, or inaccurate texture reconstruction. In contrast, our SP-MoMamba effectively preserves structural information and enhances clarity. For instance, in images img_044 and img_076 from the Urban100 dataset, SeemoRe-L Zamfir et al. (2024) and MambaIR-light Guo et al. (2024) fail to reconstruct the correct textures accurately. In contrast, our method can recover regular textures and complex details. These visual comparisons emphasize SP-MoMamba's effectiveness in reconstructing high-quality images by leveraging global information derived from superpixels. More visual results can be found in the Supplementary material.

5.3 Ablation Study

We devise a set of ablation studies to evaluate the contribution and efficacy of each proposed module. All experiments are conducted on the $\times 4$ SP-MoMamba-T setting. More ablation studies are in supplementary materials.

SP-MoMamba-T	$\#\mathcal{E}$	Scale	GMACs	BSD100	Urban100
Adding experts	1	1	22G	27.65	26.17
	2	[1,1]	26G	27.67	26.31
	3	[1,1,1]	30G	27.67	26.32
	4	[1,1,1,1]	33G	27.68	26.34
Adding scale	1	2	19G	27.63	26.11
	2	[1,2]	22G	27.68	26.33
	3	[1,2,4]	**23G**	**27.69**	**26.40**
	4	[1,2,4,8]	23G	27.67	26.24

(a) Ablation on the number of experts and corresponding scale factor.

Method	**Params**	**GMACs**	**BSD100×4**	
SP-MoMamba-T			PSNR	SSIM
k=1	271K	22.87	27.69	0.7398
k=2	271K	23.61	27.68	0.7394
k=3	271K	24.36	27.69	0.7398

(b) Ablation experiments with k values on MSS-MoE. k denotes the number of selected experts.

Table 4: Ablation on key components of MSS-MoE. We show PSNR results for ×4 upscaling.

Macro Architecture. As shown in the Table 3, we assess the effectiveness of our proposed key architectural components by comparing them against a baseline model which is composed solely of residual block. The incorporation of the proposed modules into the baseline framework yields significant enhancements in performance. Specifically, the introduction of the State Space Model (SSM) and Superpixel Sampling (SPS) lays a solid foundation, where SPS effectively reduces the computational cost (GMACs) while maintaining performance. Furthermore, the addition of the Mixture-of-Expert (MoE) strategy and Local Mixed Attention (LMA) independently augments the model's capability to capture complex features. Notably, the inclusion of the Gated Feed-Forward Network (GatedFFN) alongside these components leads to the optimal configuration (SP-MoMamba-T), which augments the baseline by 0.27 dB on BSD100 and 0.85 dB on Urban100, respectively. Although the parameter count increases moderately with the integration of all modules, the substantial performance gains validate the effectiveness of each component.

Design choices of MSS-MoE. We explore the design choices of the MSS-MoE module by varying the number of experts and their corresponding scale factor parameters, as illustrated in Table 4(a), where $\#\mathcal{E}$ denotes the number of experts. To determine the optimal number of experts and scale factors, we devise two simple scenarios: one increasing the number of experts at the same scale, and the other incorporating experts at varying scales. As evidenced in Table 4(a), employing experts across different scales outstanding enhances performance with only a modest increase in

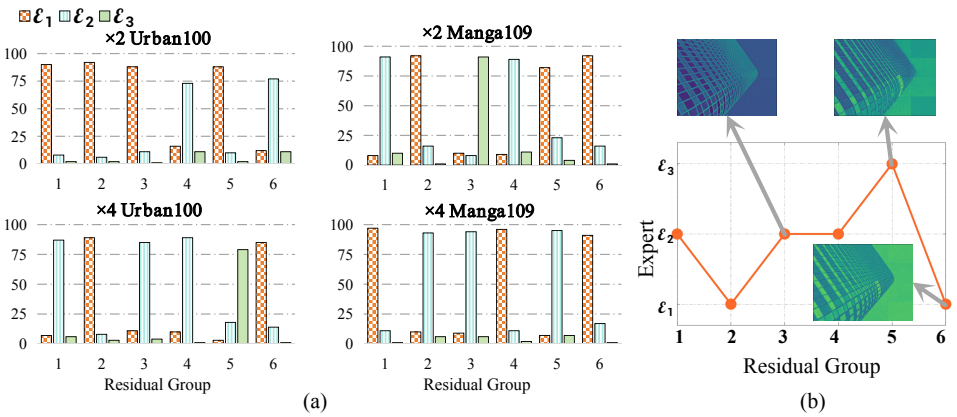

Figure 7: Expert routing analysis. (a) We plot the decisions made by the routing function for SP-MoMamba-T over the depth of the network. (b) We visualize the expert output features of SP-MoMamba-T at different scales and depth for ×4 SR given example images from Urban100.

computational cost, outperforming the method of adding experts at a uniform scale. Based on these experiments, we assert that downsampling beyond a factor of 4 results in substantial loss of semantic information, introducing much artificial information into the network and consequently degrading performance. Therefore, we select experts with scale factors of [1, 2, 4] as the final configuration. Table 4(b) analyzes the impact of parameter k. Results indicate that varying k from 1 to 3 yields negligible differences in PSNR and SSIM, yet consistently increases computational cost (GMACs). Therefore, we select $k = 1$ as the optimal setting, achieving comparable performance with minimal complexity. These results indicate that the routing mechanism effectively leverages complementary semantic information across different scales. By dynamically selecting the optimal experts via the Router, the model significantly enhances its capability for detailed reconstruction.

5.4 Discussion on Experts

The decision-making process of the router across different residual groups is illustrated in Figure 7(a). Notably, the network showcases a diverse range of expert choices ($\mathcal{E}_1, \mathcal{E}_2, \mathcal{E}_3$) across varying depths. This phenomenon can be attributed to the hierarchical feature learning nature of the architecture, aligning with our expectations. In fact, specific residual groups utilize larger scales ($\mathcal{E}_3$) to capture global dependencies, while others employ smaller scales ($\mathcal{E}_1$) to refine local details. Hence, static scales are less favored, as they may introduce redundancy or lack the capability to handle the varying complexity of features. This design aspect provides our method with the flexibility to adaptively adjust the processing scale, a capability that ensures efficiency. In Figure 7(b), we further visualize the routing decisions and corresponding feature maps for an exemplary input. It is noteworthy that the router intelligently switches between experts to leverage their distinct yet mutually complementary information. As the model depth increases, the network becomes proficient in restructuring these multi-scale representations for optimal restoration.

6 Conclusion

In this study, we propose SP-MoMamba, a superpixel-driven mixture of state space experts model. Unlike the other state space models, SP-MoMamba addresses the computational inefficiencies inherent in existing mamba-based restoration methods dependent on global scanning by integrating superpixel sampling with state space frameworks. This approach effectively balances robust global semantic modeling with precise local detail enhancement while minimizing complexity. In our method, the MSS-MoE module achieves comprehensive global modeling by dynamically selecting optimal experts across multiple scales, while the LSME refines local features through a synergistic combination of self-attention and channel attention mechanisms. Experimental results confirm that SP-MoMamba surpasses state-of-the-art lightweight models across various benchmark datasets.

Ethics Statement

We confirm that we have read and committed to complying with ICLR's ethical guidelines. This study focuses on image super-resolution technology. Although it does not directly involve human subjects, we recognize that it may be misused to generate misleading content (such as deepfakes). We are committed to responsible research and hope that this technology can be applied to beneficial fields such as medical image enhancement. All experiments are based on publicly available datasets, and we have made every effort to ensure the reproducibility and impartiality of the research.

Reproducibility Statement

To support the reproducibility of our work, we have made the following efforts. The implementation details of our proposed SP-MoMamba-T and SP-MoMamba-B architecture, including training configurations and hyperparameters, are thoroughly described in Section 5.1 and the Appendix C. The source code for the model and training scripts has been provided in our anonymized supplementary materials. Furthermore, all experiments are conducted on publicly available benchmark datasets, and the specific data preprocessing steps are clearly outlined in Section 5.1. We hope these resources will facilitate the replication of our results.

References

Radhakrishna Achanta, Appu Shaji, Kevin Smith, Aurelien Lucchi, Pascal Fua, and Sabine Süsstrunk. Slic superpixels compared to state-of-the-art superpixel methods. *IEEE transactions on pattern analysis and machine intelligence*, 34(11):2274–2282, 2012.

Namhyuk Ahn, Byungkon Kang, and Kyung-Ah Sohn. Fast, accurate, and lightweight super-resolution with cascading residual network. In *Proceedings of the European conference on computer vision (ECCV)*, pp. 252–268, 2018.

Jiesong Bai, Yuhao Yin, Qiyuan He, Yuanxian Li, and Xiaofeng Zhang. Retinexmamba: Retinex-based mamba for low-light image enhancement. In *International Conference on Neural Information Processing*, pp. 427–442. Springer, 2024.

Marco Bevilacqua, Aline Roumy, Christine Guillemot, and Marie Line Alberi-Morel. Low-complexity single-image super-resolution based on nonnegative neighbor embedding. 2012.

Yuanhao Cai, Hao Bian, Jing Lin, Haoqian Wang, Radu Timofte, and Yulun Zhang. Retinexformer: One-stage retinex-based transformer for low-light image enhancement. In *Proceedings of the IEEE/CVF international conference on computer vision*, pp. 12504–12513, 2023.

Zheng Chen, Yulun Zhang, Jinjin Gu, Linghe Kong, Xiaokang Yang, and Fisher Yu. Dual aggregation transformer for image super-resolution. In *Proceedings of the IEEE/CVF international conference on computer vision*, pp. 12312–12321, 2023.

Xiangxiang Chu, Bo Zhang, Hailong Ma, Ruijun Xu, and Qingyuan Li. Fast, accurate and lightweight super-resolution with neural architecture search. In *2020 25th International conference on pattern recognition (ICPR)*, pp. 59–64. IEEE, 2021.

Marcos V Conde, Ui-Jin Choi, Maxime Burchi, and Radu Timofte. Swin2sr: Swinv2 transformer for compressed image super-resolution and restoration. In *European Conference on Computer Vision*, pp. 669–687. Springer, 2022.

Tao Dai, Jianping Wang, Hang Guo, Jinmin Li, Jinbao Wang, and Zexuan Zhu. Freqformer: Frequency-aware transformer for lightweight image super-resolution. In *Proceedings of the International Joint Conference on Artificial Intelligence*, pp. 731–739, 2024.

Chao Dong, Chen Change Loy, Kaiming He, and Xiaoou Tang. Image super-resolution using deep convolutional networks. *IEEE transactions on pattern analysis and machine intelligence*, 38(2): 295–307, 2015.

Mohammad Emad, Maurice Peemen, and Henk Corporaal. Moesr: Blind super-resolution using kernel-aware mixture of experts. In *Proceedings of the IEEE/CVF Winter Conference on Applications of Computer Vision*, pp. 3408–3417, 2022.

Albert Gu and Tri Dao. Mamba: Linear-time sequence modeling with selective state spaces. *arXiv preprint arXiv:2312.00752*, 2023.

Hang Guo, Jinmin Li, Tao Dai, Zhihao Ouyang, Xudong Ren, and Shu-Tao Xia. Mambair: A simple baseline for image restoration with state-space model. In *European conference on computer vision*, pp. 222–241. Springer, 2024.

Hang Guo, Yong Guo, Yaohua Zha, Yulun Zhang, Wenbo Li, Tao Dai, Shu-Tao Xia, and Yawei Li. Mambairv2: Attentive state space restoration. In *Proceedings of the Computer Vision and Pattern Recognition Conference*, pp. 28124–28133, 2025.

Feng Huang, Hongwei Liu, Liqiong Chen, Ying Shen, and Min Yu. Feature enhanced cascading attention network for lightweight image super-resolution. *Scientific Reports*, 15(1):2051, 2025.

Huaibo Huang, Xiaoqiang Zhou, Jie Cao, Ran He, and Tieniu Tan. Vision transformer with super token sampling. *arXiv preprint arXiv:2211.11167*, 2022.

J. Huang, A. Singh, and N. Ahuja. Single image super-resolution from transformed self-exemplars. In *2015 IEEE Conference on Computer Vision and Pattern Recognition (CVPR)*, pp. 5197–5206, 2015. doi: 10.1109/CVPR.2015.7299156.

Zheng Hui, Xiumei Wang, and Xinbo Gao. Fast and accurate single image super-resolution via information distillation network. In *Proceedings of the IEEE conference on computer vision and pattern recognition*, pp. 723–731, 2018.

Varun Jampani, Deqing Sun, Ming-Yu Liu, Ming-Hsuan Yang, and Jan Kautz. Superpixel sampling networks. In *Proceedings of the European Conference on Computer Vision (ECCV)*, pp. 352–368, 2018.

Eric Jang, Shixiang Gu, and Ben Poole. Categorical reparameterization with gumbel-softmax. *arXiv preprint arXiv:1611.01144*, 2016.

Diederik P Kingma and Jimmy Ba. Adam: A method for stochastic optimization. *arXiv preprint arXiv:1412.6980*, 2014.

Ao Li, Le Zhang, Yun Liu, and Ce Zhu. Exploring frequency-inspired optimization in transformer for efficient single image super-resolution. *IEEE Transactions on Pattern Analysis and Machine Intelligence*, 2025a.

Chongyi Li, Chun-Le Guo, Man Zhou, Zhexin Liang, Shangchen Zhou, Ruicheng Feng, and Chen Change Loy. Embedding fourier for ultra-high-definition low-light image enhancement. *arXiv preprint arXiv:2302.11831*, 2023a.

Feng Li, Runmin Cong, Jingjing Wu, Huihui Bai, Meng Wang, and Yao Zhao. Srconvnet: A transformer-style convnet for lightweight image super-resolution. *International Journal of Computer Vision*, 133(1):173–189, 2025b.

Yawei Li, Yuchen Fan, Xiaoyu Xiang, Denis Demandolx, Rakesh Ranjan, Radu Timofte, and Luc Van Gool. Efficient and explicit modelling of image hierarchies for image restoration. In *Proceedings of the IEEE/CVF Conference on Computer Vision and Pattern Recognition (CVPR)*, pp. 18278–18289, June 2023b.

Jie Liang, Hui Zeng, and Lei Zhang. Efficient and degradation-adaptive network for real-world image super-resolution. In *European Conference on Computer Vision*, pp. 574–591. Springer, 2022.

Jingyun Liang, Jiezhang Cao, Guolei Sun, Kai Zhang, Luc Van Gool, and Radu Timofte. Swinir: Image restoration using swin transformer. In *Proceedings of the IEEE/CVF international conference on computer vision*, pp. 1833–1844, 2021.

B. Lim, S. Son, H. Kim, S. Nah, and K. M. Lee. Enhanced deep residual networks for single image super-resolution. In *2017 IEEE Conference on Computer Vision and Pattern Recognition Workshops (CVPRW)*, pp. 1132–1140, 2017. doi: 10.1109/CVPRW.2017.151.

Jie Liu, Jie Tang, and Gangshan Wu. Residual feature distillation network for lightweight image super-resolution. In *Computer vision–ECCV 2020 workshops: Glasgow, UK, August 23–28, 2020, proceedings, part III 16*, pp. 41–55. Springer, 2020.

Yue Liu, Yunjie Tian, Yuzhong Zhao, Hongtian Yu, Lingxi Xie, Yaowei Wang, Qixiang Ye, and Yunfan Liu. Vmamba: Visual state space model. *arXiv preprint arXiv:2401.10166*, 2024.

Zhisheng Lu, Juncheng Li, Hong Liu, Chaoyan Huang, Linlin Zhang, and Tieyong Zeng. Transformer for single image super-resolution. In *Proceedings of the IEEE/CVF conference on computer vision and pattern recognition*, pp. 457–466, 2022.

D. Martin, C. Fowlkes, D. Tal, and J. Malik. A database of human segmented natural images and its application to evaluating segmentation algorithms and measuring ecological statistics. In *Proceedings Eighth IEEE International Conference on Computer Vision. ICCV 2001*, volume 2, pp. 416–423 vol.2, 2001. doi: 10.1109/ICCV.2001.937655.

Yusuke Matsui, Kota Ito, Yuji Aramaki, Toshihiko Yamasaki, and Kiyoharu Aizawa. Sketch-based manga retrieval using manga109 dataset. 2015.

Karam Park, Jae Woong Soh, and Nam Ik Cho. A dynamic residual self-attention network for lightweight single image super-resolution. *IEEE Transactions on Multimedia*, 25:907–918, 2021.

Junbo Qiao, Jincheng Liao, Wei Li, Yulun Zhang, Yong Guo, Yi Wen, Zhangxizi Qiu, Jiao Xie, Jie Hu, and Shaohui Lin. Hi-mamba: Hierarchical mamba for efficient image super-resolution. *arXiv preprint arXiv:2410.10140*, 2024.

Carlos Riquelme, Joan Puigcerver, Basil Mustafa, Maxim Neumann, Rodolphe Jenatton, André Susano Pinto, Daniel Keysers, and Neil Houlsby. Scaling vision with sparse mixture of experts. *Advances in Neural Information Processing Systems*, 34:8583–8595, 2021.

Leonardo Rossi, Vittorio Bernuzzi, Tomaso Fontanini, Massimo Bertozzi, and Andrea Prati. Swin2-mose: A new single image supersolution model for remote sensing. *IET Image Processing*, 19 (1):e13303, 2025.

Noam Shazeer. Glu variants improve transformer. *arXiv preprint arXiv:2002.05202*, 2020.

Long Sun, Jinshan Pan, and Jinhui Tang. Shufflemixer: An efficient convnet for image super-resolution. *Advances in Neural Information Processing Systems*, 35:17314–17326, 2022.

Long Sun, Jiangxin Dong, Jinhui Tang, and Jinshan Pan. Spatially-adaptive feature modulation for efficient image super-resolution. In *Proceedings of the IEEE/CVF international conference on computer vision*, pp. 13190–13199, 2023.

Ying Tai, Jian Yang, and Xiaoming Liu. Image super-resolution via deep recursive residual network. In *Proceedings of the IEEE conference on computer vision and pattern recognition*, pp. 3147–3155, 2017.

R. Timofte, E. Agustsson, L. V. Gool, M. Yang, L. Zhang, B. Lim, S. Son, H. Kim, S. Nah, and K. M. Lee et al. Ntire 2017 challenge on single image super-resolution: Methods and results. In *2017 IEEE Conference on Computer Vision and Pattern Recognition Workshops (CVPRW)*, pp. 1110–1121, 2017. doi: 10.1109/CVPRW.2017.149.

Cong Wang, Jinshan Pan, Wei Wang, Gang Fu, Siyuan Liang, Mengzhu Wang, Xiao-Ming Wu, and Jun Liu. Correlation matching transformation transformers for uhd image restoration. In *Proceedings of the AAAI Conference on Artificial Intelligence*, volume 38, pp. 5336–5344, 2024a.

Yan Wang, Yi Liu, Shijie Zhao, Junlin Li, and Li Zhang. Camixersr: Only details need more" attention". In *Proceedings of the IEEE/CVF Conference on Computer Vision and Pattern Recognition*, pp. 25837–25846, 2024b.

Zeyu Wang, Chen Li, Huiying Xu, and Xinzhong Zhu. Mamba yolo: Ssms-based yolo for object detection. *arXiv preprint arXiv:2406.05835*, 2024c.

Jiangwei Weng, Zhiqiang Yan, Ying Tai, Jianjun Qian, Jian Yang, and Jun Li. Mamballie: Implicit retinex-aware low light enhancement with global-then-local state space. *Advances in Neural Information Processing Systems*, 37:27440–27462, 2024.

Lemeng Wu, Mengchen Liu, Yinpeng Chen, Dongdong Chen, Xiyang Dai, and Lu Yuan. Residual mixture of experts. *arXiv preprint arXiv:2204.09636*, 2022.

Qingsen Yan, Kangbiao Shi, Yixu Feng, Tao Hu, Peng Wu, Guansong Pang, and Yanning Zhang. Hvi-cidnet+: Beyond extreme darkness for low-light image enhancement. *arXiv preprint arXiv:2507.06814*, 2025.

Eduard Zamfir, Zongwei Wu, Nancy Mehta, Yulun Zhang, and Radu Timofte. See more details: Efficient image super-resolution by experts mining. In *Forty-first International Conference on Machine Learning*, 2024.

Roman Zeyde, Michael Elad, and Matan Protter. On single image scale-up using sparse-representations. 2010.

Aiping Zhang, Wenqi Ren, Yi Liu, and Xiaochun Cao. Lightweight image super-resolution with superpixel token interaction. In *Proceedings of the IEEE/CVF international conference on computer vision*, pp. 12728–12737, 2023.

Guowen Zhang, Lue Fan, Chenhang He, Zhen Lei, ZHAO-XIANG ZHANG, and Lei Zhang. Voxel mamba: Group-free state space models for point cloud based 3d object detection. *Advances in Neural Information Processing Systems*, 37:81489–81509, 2025a.

Tongshun Zhang, Pingping Liu, Ming Zhao, and Haotian Lv. Dmfourllie: dual-stage and multi-branch fourier network for low-light image enhancement. In *Proceedings of the 32nd ACM International Conference on Multimedia*, pp. 7434–7443, 2024.

Tongshun Zhang, Pingping Liu, Yubing Lu, Mengen Cai, Zijian Zhang, Zhe Zhang, and Qiuzhan Zhou. Cwnet: Causal wavelet network for low-light image enhancement. In *Proceedings of the IEEE/CVF International Conference on Computer Vision*, pp. 8789–8799, 2025b.

Xindong Zhang, Hui Zeng, Shi Guo, and Lei Zhang. Efficient long-range attention network for image super-resolution. In *European conference on computer vision*, pp. 649–667. Springer, 2022.

Yulun Zhang, Kunpeng Li, Kai Li, Lichen Wang, Bineng Zhong, and Yun Fu. Image super-resolution using very deep residual channel attention networks. In *Proceedings of the European conference on computer vision (ECCV)*, pp. 286–301, 2018.

Hengyuan Zhao, Xiangtao Kong, Jingwen He, Yu Qiao, and Chao Dong. Efficient image super-resolution using pixel attention. In *Computer Vision–ECCV 2020 Workshops: Glasgow, UK, August 23–28, 2020, Proceedings, Part III 16*, pp. 56–72. Springer, 2020.

Zou Zhen, Yu Hu, and Zhao Feng. Freqmamba: Viewing mamba from a frequency perspective for image deraining. *arXiv preprint arXiv:2404.09476*, 2024.

Yupeng Zhou, Zhen Li, Chun-Le Guo, Song Bai, Ming-Ming Cheng, and Qibin Hou. Srformer: Permuted self-attention for single image super-resolution. In *Proceedings of the IEEE/CVF International Conference on Computer Vision*, pp. 12780–12791, 2023.

Lianghui Zhu, Bencheng Liao, Qian Zhang, Xinlong Wang, Wenyu Liu, and Xinggang Wang. Vision mamba: Efficient visual representation learning with bidirectional state space model. *arXiv preprint arXiv:2401.09417*, 2024.

Wenbin Zou, Tian Ye, Weixin Zheng, Yunchen Zhang, Liang Chen, and Yi Wu. Self-calibrated efficient transformer for lightweight super-resolution. In *Proceedings of the IEEE/CVF conference on computer vision and pattern recognition*, pp. 930–939, 2022.

Wenbin Zou, Hongxia Gao, Weipeng Yang, and Tongtong Liu. Wave-mamba: Wavelet state space model for ultra-high-definition low-light image enhancement. In *Proceedings of the 32nd ACM International Conference on Multimedia*, pp. 1534–1543, 2024.

APPENDIX

In this Appendix, we declare The Use of Large Language Models (LLMs). In addition, we present the principle of state space model and provide implementation details, additional experimental results and analysis.

A THE USE OF LARGE LANGUAGE MODELS (LLMS)

A large language model was used during the preparation of this work solely for text polishing and grammar correction. The authors are solely responsible for the entire scientific content, including all ideas, findings, and interpretations presented herein.

B STATE SPACE MODELS

State space models (SSMs) Gu & Dao (2023) are mathematical models used in control theory and signal processing to describe the dynamic systems. The following equation defines the standard SSMs:

$$h'(t) = \mathbf{A}h(t) + \mathbf{B}x(t) \tag{10}$$

$$y(t) = \mathbf{C}h(t) + \mathbf{D}x(t) \tag{11}$$

where $\mathbf{A}, \mathbf{B}, \mathbf{C}$, and $\mathbf{D}$ are the system parameters. $x(t), h(t)$ and $y(t)$ denote input, hidden state, and output. In deep learning, the existing SSM-based methods, like Mamba, employ zero-order hold (ZOH) to discretize continuous state space equations, enabling them to efficiently process long sequence data and apply to various sequence modeling tasks. It is represented by the following equations:

Parameters	SP-MoMamba-T	SP-MoMamba-S
Num. RGs	3	4
Num. SGMEs and LSMEs	2	2
Channel dimension	36	48
MLP-Ratio	2	
Num. superpixels	64	
Num. Experts $\mathcal{E}$	3	
Top-k experts	1	
Scale list	[1,2,4]	
Training Dataset	DIV2K+Flickr2K	
Optimizer	Adam	
Batch size	32	
Total Num. Iterations	500K	
FFT Loss weights	0.1	
LR-Rate	1.00E-03	
LR-Decay Rate	0.5	
LR-Decay Milestones	[250K,400K, 450K, 475K]	

Table 5: Implementation Details.

$$h_t = \bar{\mathbf{A}}h_{t-1} + \bar{\mathbf{B}}x_t \tag{12}$$

$$y_t = \mathbf{C}h_t + \mathbf{D}x_t \tag{13}$$

$$\bar{\mathbf{A}} = \exp(\Delta\mathbf{A}) \tag{14}$$

$$\bar{\mathbf{B}} = (\Delta\mathbf{A})^{-1}(\exp(\Delta\mathbf{A}) - \mathbf{I})(\Delta\mathbf{B}) \tag{15}$$

where $\bar{\mathbf{A}}, \bar{\mathbf{B}}$ are discrete counterparts of $\mathbf{A}$ and $\mathbf{B}$. $\mathbf{\Delta}$ denotes timescale parameter, which is used to convert the continuous parameters $\mathbf{A}$ and $\mathbf{B}$ into discrete ones $\bar{\mathbf{A}}$, and $\bar{\mathbf{B}}$.

C FURTHER IMPLEMENTATION DETAILS

Table 5 details the architectural configurations and training parameters utilized to obtain the results presented in this study. To ensure reproducibility, we maintained a consistent random seed across all experiments. Our implementation leverages the publicly available PyTorch-based BasicSR framework for both architecture design and training. Additionally, we employ the fvcore Python package to calculate GMACs and parameter counts. The pseudocode for the proposed MSS-MoE is provided in Algorithm 1.

Algorithm 1 Multi-Scale Superpixel Mixture of State space Experts (MSS-MoE)

Input: Input feature x_1 and x_2
Parameters: n experts $\mathcal{E}$, Router $\mathcal{G}$, Scale factor $s = s_1, s_2, ..., s_n$, Superpixel state space module (SP-SSM), Top-k expert
Compute router outputs: $g = \mathcal{G}(x_2)$
Normalize weights: $w = \text{Softmax}(g)$
Select top-k expert: $w_{\text{top-}k} = \text{topk}(w, k)$
Set all other weights to zero: $w_i = 0$ for $i \neq$ top-k
if training **then**
  for each $i \in \mathcal{E}$ **do**
    $y_i = \text{SP-SSM}(x_1, s_i) \odot \sigma(x_2)$
  end for
  Compute final output: $y = \sum_{i=1}^{n} w_i \cdot y_i$
else
  Compute final output: $y = w_{\text{top-}k} \cdot y_{\text{top-}k}$
end if
Output: Final output y

C.1 Comparison to lightweight SR mdoels (×3).

In Table 6, 7, we present the performance of our SP-MoMamba-T and SP-MoMamba-B model for $\times 3$ upscaling, extending the results from Table 1, 2 in the main text. Our SP-MoMamba-T and SP-MoMamba-B can achieve competitive performance with lower parameter and computational complexity.

Scale	Model	Params (M)↓	GMACs↓	Set5		Set14		BSD100		Urban100		Manga109	
				PSNR↑	SSIM↑	PSNR↑	SSIM↑	PSNR↑	SSIM↑	PSNR↑	SSIM↑	PSNR↑	SSIM↑
×3	CARN-M	415K	46	33.99	0.9236	30.08	0.8367	28.91	0.8000	27.55	0.8385	—	—
	PAN	261K	39	34.40	0.9271	30.36	0.8423	29.11	0.8050	28.11	0.8511	33.61	0.9448
	DRSAN	410K	43	34.41	0.9272	30.27	0.8413	29.08	0.8056	28.19	0.8529	—	—
	SAFMN	233K	23	34.34	0.9270	30.33	0.8418	29.08	0.8048	27.95	0.8474	33.52	0.9437
	SeemoRe-T	225K	20	<u>34.46</u>	<u>0.9276</u>	<u>30.44</u>	<u>0.8445</u>	<u>29.15</u>	<u>0.8063</u>	<u>28.27</u>	<u>0.8538</u>	<u>33.92</u>	<u>0.9460</u>
	SRConvNet	387K	33	34.40	0.9272	30.30	0.8416	29.07	0.8500	28.04	0.8474	33.56	0.9443
	SP-MoMamba-T (ours)	264K	37	**34.53**	**0.9284**	**30.50**	**0.8448**	**29.19**	**0.8080**	**28.43**	**0.8572**	**34.16**	**0.9504**

Table 6: Comparison to efficient SR models. PSNR (dB ↑) and SSIM (↑) metrics are reported on the Y-channel. **Best** and <u>second best</u> performances are highlighted. GMACs (G) are computed by upscaling to a 1280 × 720 HR image.

scale	Model	Params (M)	GMACs	Set5		Set14		BSD100		Urban100		Manga109	
				PSNR	SSIM	PSNR	SSIM	PSNR	SSIM	PSNR	SSIM	PSNR	SSIM
×3	SwinIR-Light	918K	111	34.62	0.9289	30.54	0.8463	29.20	0.8082	28.66	0.8624	33.98	0.9478
	SRFormer-Light	861K	105	34.67	0.9296	30.57	0.8469	29.26	0.8099	28.81	0.8655	34.19	0.9489
	SPIN	569K	176	34.65	0.9293	30.57	0.8464	29.23	0.8089	28.71	0.8627	34.24	0.9489
	MambaIR-light	913K	149	34.63	0.9288	30.54	0.8459	29.23	0.8084	28.70	0.8631	34.12	0.9479
	SeemoRe-L	959K	87	34.70	<u>0.9297</u>	30.60	0.8469	29.29	<u>0.8101</u>	<u>28.86</u>	<u>0.8653</u>	<u>34.53</u>	<u>0.9496</u>
	CRAFT	744K	88	34.71	0.9295	30.61	0.8469	29.24	0.8093	28.77	0.8635	34.29	0.9491
	MambaIRv2-light	781K	127	<u>34.71</u>	0.9297	**30.68**	**0.8483**	<u>29.26</u>	0.8098	**29.01**	**0.8689**	34.41	0.9497
	SP-MoMamba-B (ours)	550K	75	**34.71**	**0.9297**	<u>30.65</u>	<u>0.8478</u>	**29.29**	**0.8104**	28.84	0.8652	**34.67**	**0.9530**

Table 7: Comparison to lightweight SR models. PSNR (dB ↑) and SSIM (↑) metrics are reported on the Y-channel. **Best** and <u>second best</u> performances are highlighted. GMACs (G) are computed by upscaling to a 1280 × 720 HR image.

C.2 Evaluation on Real SR

We conduct experiments for Real SR ($\times 4$) using the Real-ESRGAN degradation model to evaluate SP-MoMamba-T against current efficient SOTA SR models such as SAFMN, SPIN, and SeemoRe-T, see Table 8. We report the popular NR-IQA metrics (NIQE and BRISQUE) on the commonly used real-world image collection provided by SeemoRe. As illustrated in the results, our method achieves the lowest scores (6.42 in NIQE and 44.69 in BRISQUE), indicating superior perceptual quality. Additionally, we conduct a cross-dataset evaluation using testsets with more realistic degradation of different severity levels (DIV2K-I and DIV2K-II). In these quantitative comparisons re-

Method	NIQE↓	BRISQUE↓	DIV2K-I (PSNR↑)	DIV2K-II (PSNR↑)
Bicubic	7.65	58.29	26.30	25.71
SAFMN	7.19	51.39	26.80	26.77
SPIN	6.84	58.27	26.93	26.86
SeemoRe-T	6.53	45.53	27.07	27.01
SP-MoMamba-T	6.42	44.69	27.13	27.09

Table 8: Real SR performance. NIQE and BRISQUE are reported on the real image collection provided by SeemoRe. DIV2K-I and DIV2K-II performance reported as PSNR.

Method	**LOLv1**		**LOLv2-Real**	
	PSNR ↑	**SSIM ↑**	**PSNR ↑**	**SSIM ↑**
UHDFourLi et al. (2023a)	22.89	0.8147	19.42	0.7896
RetinexformerCai et al. (2023)	22.71	0.8177	22.79	0.8397
DMFourLLIE Zhang et al. (2024)	22.98	0.8273	22.71	0.8583
UHDFormer Wang et al. (2024a)	22.88	0.8370	19.71	0.832
RetinexMamba Bai et al. (2024)	23.15	0.8210	21.73	0.829
MambaLLIE Weng et al. (2024)	22.80	0.8315	21.85	0.8276
CWNet Zhang et al. (2025b)	23.60	0.8496	23.31	0.8641
CIDNet Yan et al. (2025)	23.81	**0.8574**	**23.43**	0.8622
SP-MoMamba-T	23.25	0.8570	24.23	0.8732

Table 9: Analysis of SP-MoMamba generalization. We provide a performance comparison of SP-MoMamba on low-light image enhancement task.

ported as PSNR, SP-MoMamba-T consistently outperforms the competing methods, demonstrating its robustness in handling complex real-world degradation.

C.3 Evaluation on low-light image enhancement

As shown in Table 9, we assess the generalization capability of our proposed method by extending its application to the low-light image enhancement task. We compare SP-MoMamba-T against comprehensive state-of-the-art approaches, including Transformer-based (e.g., Retinexformer) and CNN-based (e.g., CIDNet) methods on the LOLv1 and LOLv2-Real datasets. Notably, our model yields significant enhancements, particularly on the more challenging LOLv2-Real benchmark. Specifically, SP-MoMamba-T outperforms the second-best method, CIDNet, achieving pronounced improvements of 0.80 dB in PSNR and 0.011 in SSIM. This phenomenon can be attributed to the robust global modeling capability of our superpixel-based architecture, which effectively restores illumination while preserving structural details. Overall, these advancements culminate in superior performance metrics, underscoring the flexibility and strong generalization potential of our design beyond the super-resolution task.

Method	Time (s)	GPU Memory	PSNR
SwinIR-Light	0.631	6802.7	30.91
SRFormer-Light	0.734	7319.4	31.17
SPIN	0.654	7083	30.98
Mambairv2-Light	0.833	13652.3	31.24
CATANet	0.745	21962	31.31
SeemoRe-L	0.145	10464.7	31.48
SP-MoMamba-T	**0.084**	**4258.1**	31.01
SP-MoMamba-B	0.236	6572.9	**31.51**

Table 10: Comparison between performance vs Inference times and GPU Memory on Manga109 ×4 dataset. Inference times and GPU Memory are calculated on 720p HR image.

C.4 Detailed comparison of model complexity

We provide a detailed comparison of memory usage and runtime as shown in Table 10. From the table, it can be seen that compared to the current best method, our SP-MoMamba-T has lowest inference time and GPU memory, and achieves more competitive performance.

D More Ablations

D.1 Ablation for LMA.

As a core component of the LSME module, the Local Mixed Attention (LMA) employs diverse strategies for focusing on local information, thereby effectively enhancing localized feature representation. Table 11 demonstrates that window multi-head self-attention (Swin MHSA) Liang et al. (2021), owing to its efficient window-based self-attention mechanism, achieves superior performance compared to the channel attention (CA) mechanism Zhang et al. (2018). However, Swin MHSA is restricted to spatially capturing local information, overlooking similarity relationships between different channels. Consequently, integrating CA with Swin MHSA can significantly enhance local features, leading to finer textures and improved performance. As demonstrated in Table 11, with the incorporation of CA and Swin MHSA, the model achieves optimal performance.

Method	Params	GMACs	BSD100	Urban100
Swin MHSA	224K	20	27.67	26.28
CA	240K	13	27.65	25.22
LMA	271K	22	**27.69**	**26.40**

Table 11: Ablation on the Local Mixed Attention (LMA) mechanism. We show results for $\times 4$ upscaling.

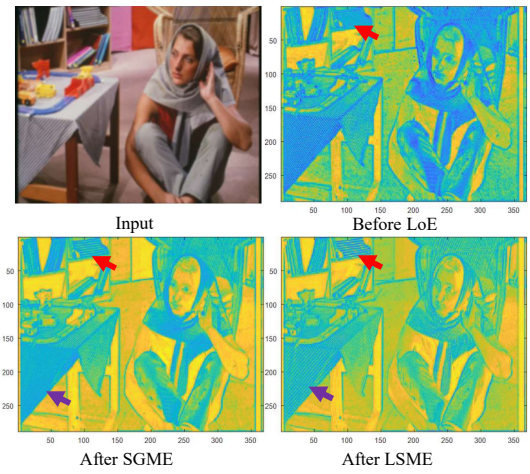

Figure 8: Visualizations of feature maps before and after applying the proposed SGME and LSME modules, demonstrating enhanced activation sharpness through SGME and refined representations via LSME. (Zoom in for the best view)

D.2 Ablation For Superpixel Sampling

We quantitatively compared our approach against hard clustering (SLIC) and learnable token pooling (e.g., STA). As shown in Table 12, our SSN-based strategy exhibits superior convergence and

Method	Params	GMACs	BSD100	Urban100
SP-MoMamba-T				
w SLIC Achanta et al. (2012)	271K	26	27.51	26.03
w STA Huang et al. (2022)	460K	38	27.72	26.49
w SSN (Ours)	271K	22	27.69	26.30

Table 12: Superpixel sampling method. We compared the performance impact of different superpixel sampling method separately.

Method	aggregation method	Urban100	Manga109
SP-MoMamba-T	w/o gate mechanism	32.11	38.96
	w add	32.15	38.99
	w gate mechanism	32.22	39.01

Table 13: Analysis of gating Mechanism on SP-SSM. We provide further insights in the design decisions of our SP-MoMamba-T framework for ×2 upscaling.

numerical stability compared to token pooling methods, which often suffer from token collapse. This confirms that our differentiable clustering provides a more robust foundation for the pipeline.

D.3 The Impact of Gate Control Mechanism on Performance in SP-SSM

As evidenced in Table 13, removing the gating module or replacing it with element-wise addition results in performance degradation. This quantitatively confirms that the gating mechanism is indispensable for the model's reconstruction capability.

D.4 Feature Visualization.

To substantiate the importance of the proposed SGME and LSME modules, we analyzed the feature maps before and after their integration into the Layer of Experts (LoEs), as illustrated in Figure 11. This analysis vividly highlights the strengths of employing MSS-MoE within the SGME module for global information extraction and the advantages of utilizing Swin MHSA combined with CA in the LSME module for local information refinement. Specifically, as indicated by the red arrows, structural global textures are markedly enhanced in the SGME module and subsequently refined further in the LSME module. Notably, as shown by the purple arrows, textures lost during the SGME filtering process are effectively recovered and complemented in the LSME stage, thereby synergistically enhancing the feature representation.

Method	experts	Num superpixels	GMACs	BSD100	Urban100
SP-MoMmaba-T	3	**[64,64,64]**	22	**27.69**	**26.40**
	3	[16,32,64]	**21**	27.65	26.28
	3	[32,64,128]	39	27.66	26.30

Table 14: Analysis of the impact of the number of superpixels on the performance of MSS-MoE.

D.5 Number of Superpixel on MSS-MoE

Since superpixels represent the most relevant pixels within the same semantic region, a higher number of superpixels leads to finer semantic segmentation. To further investigate the impact of superpixel quantity on the performance of MSS-MoE, we conducted a series of ablation experiments, as presented in Table 14. The results indicate that increasing the number of superpixels does not necessarily yield better performance; it has minimal impact on network accuracy but noticeably affects computational efficiency. This stems from the fact that a greater number of superpixels merely subdivides identical semantic regions without capturing semantic information across different scales. Consequently, incorporating multi-scale superpixels proves more effective in enhancing model performance.

Method	L1	FFT	BSD100	Urban100
SP-MoMmaba-T	1.0	0.0	27.65	26.26
	1.0	**0.1**	**27.69**	**26.40**
	1.0	0.2	27.68	26.32

Table 15: Loss function. SP-MoMamba was trained on DIV2K and Flickr2K. We report PSNR (dB ↑) on the Y-Channel for ×4 upscaling.

D.6 Loss Function

We use FFT loss and L1 loss to jointly optimize the network. The specific expression is as follows:

$$L_{total} = L_1 + w * L_{FFT} \tag{16}$$

$$L_1 = ||I_{gt} - I_{SR}||_1 \tag{17}$$

$$L_{FFT} = ||FFT(I_{gt}) - FFT(I_{SR})||_1 \tag{18}$$

where the $FFT(\cdot)$ denotes the Fourier Transformation. The I_{gt} and I_{SR} represent the ground-truth image and super-resolution image. To verify the effectiveness of the loss function, we designed a group of ablation experiments, as shown in Table 15. As can be seen from the table, compared with using only L1 loss, the added FFT loss can effectively add constraints in the frequency domain to the model, so as not to over smooth the texture and make the performance better.

E Visual Results

In Figure 9, we provide additional visual comparisons for the BSD100 benchmark, and in Figure 10 for the Urban100 benchmark ($\times 4$). Our SP-MoMamba framework consistently delivers visually appealing results, even when applied to intricate architectural structures. For example, as demonstrated by img021 in Figure 9, our model significantly outperforms other methods in reconstructing patterns with greater fidelity. Moreover, the reconstruction of img096 in Figure 10 exhibits reduced blur and sharper edges, thereby improving overall visual clarity.

We also provide additional the LAM results and Diffusion Index (DI) in Figure 11. It validates semantic preservation in natural scenes containing discrete, similarly textured objects. While MambaIR and MambaIRv2 display localized activation, failing to link spatially separated instances, SP-MoMamba demonstrates broader coverage by effectively leveraging information from neighboring objects. This superior capture of non-local correlations is quantitatively confirmed by the highest DI score of 24.36 (vs. 19.28/23.91), proving our method overcomes 1D scanning limitations to maintain semantic integrity.

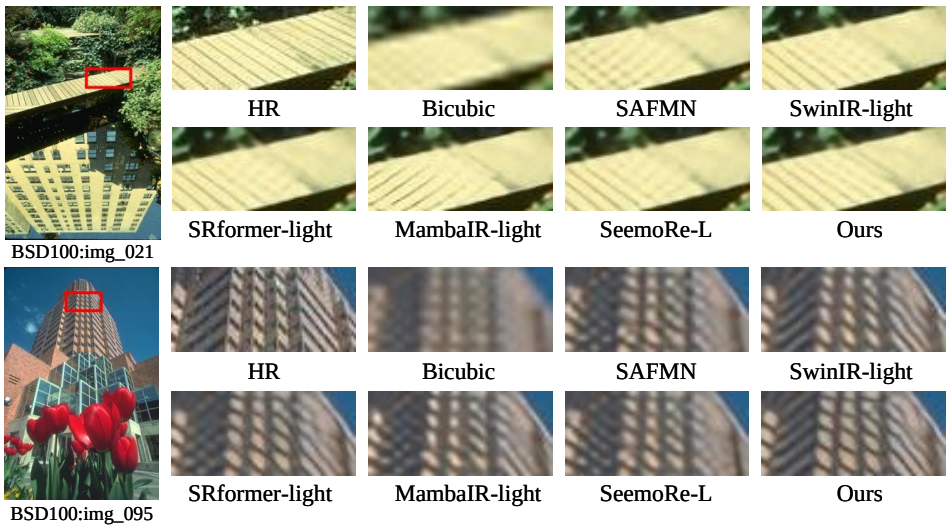

Figure 9: Visual comparison of SP-MoMamba with state-of-the-art methods on challenging cases for ×4 SR from the BSD100 benchmark

F Failure Cases and Limitation

Despite the impressive balance between efficiency and performance achieved by our proposed SP-MoMamba, we acknowledge certain limitations inherent to our design. As illustrated in the failure case in the Figure 12, the model encounters difficulties when reconstructing scenes containing

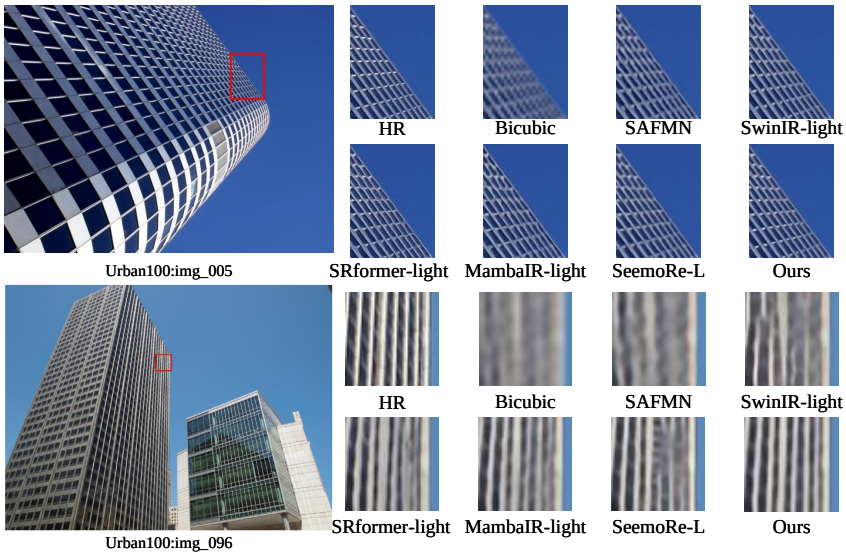

Figure 10: Visual comparison of SP-MoMamba with state-of-the-art methods on challenging cases for ×4 SR from the Urban100 benchmark

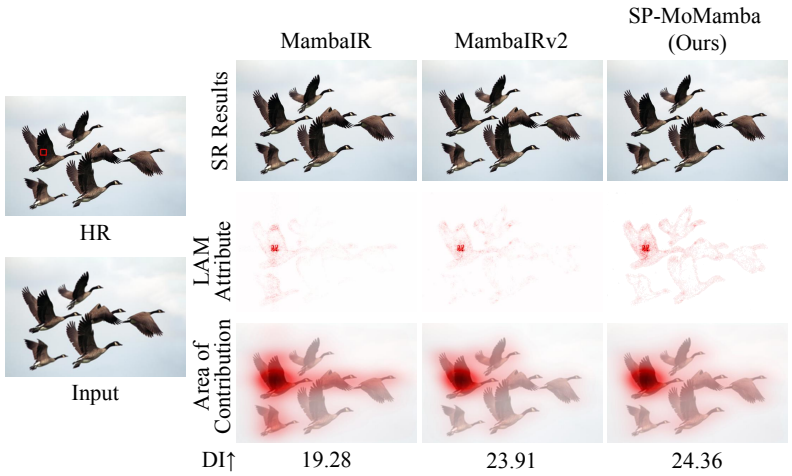

Figure 11: Analysis semantic preservation capability of different methods. The larger the Diffusion Index (DI), the more semantically similar pixels are involved in restoring the corresponding region. (Zoom in for the best view)

extremely dense, high-frequency repetitive patterns under severe degradation. Notably, while our method recovers sharper edges compared to competing models like Mambairv2-light, it inadvertently introduces slight geometric distortions and aliasing artifacts within the fine grid structures. This phenomenon can be attributed to the dependency on superpixel-guided priors; our core motivation employs superpixels to maintain semantic structure and mitigate the semantic destruction typically caused by traditional Mamba scanning. However, when dealing with extremely blurry or noisy low-resolution inputs, superpixel algorithms may struggle to generate semantic regions with precise edge alignment. In fact, this geometric inaccuracy serves to mislead the subsequent State Space Models (SSM), thereby affecting the fidelity of the final reconstruction results. Consequently, while the global semantic layout is preserved, the local high-frequency precision is compromised in these extreme scenarios.

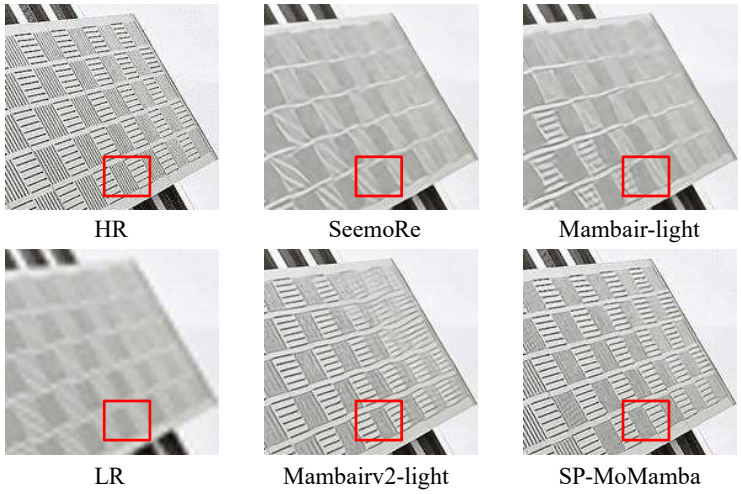

Figure 12: Visual comparison of SP-MoMamba with state-of-the-art methods on challenging cases for ×4 SR from the Urban100 benchmark